Supplementary Information

Development of a STEAP1-Targeted Prostate Cancer Specific Antibody Drug Conjugate Platform with Immunostimulatory Properties

John S. Wang[1], Sirajbir Sodhi[2], Li-Chung Tsao[3], Guang Han Lin[4], Nicole Moon[3], Qiang Zhang[5], Bushangqing Liu[3], Juliet Penaranda[3], Timothy Trotter[3], Jason Somarelli[2,6], Andrew J. Armstrong[2,6], H. Kim Lyerly[3,6], Guangdi Wang[5], and Zachary C. Hartman[3,6*]

[1]Medical Sciences Training Program, Duke University, Durham, NC, USA

[2]Department of Medicine, Duke University, Durham, NC, USA

[3]Department of Surgery, Duke University, Durham, NC, USA

[4]Department of Pharmacology and Cancer Biology, Durham, NC, USA

[5]Department of Chemistry, Xavier University, New Orleans, LA, USA

[6]Duke Cancer Institute, Duke University, Durham, NC, USA

*corresponding author. Email: zachary.hartman@duke.edu

Supplementary Information includes:

Supplementary Figures S1 to S6.

Supplementary Figure 1

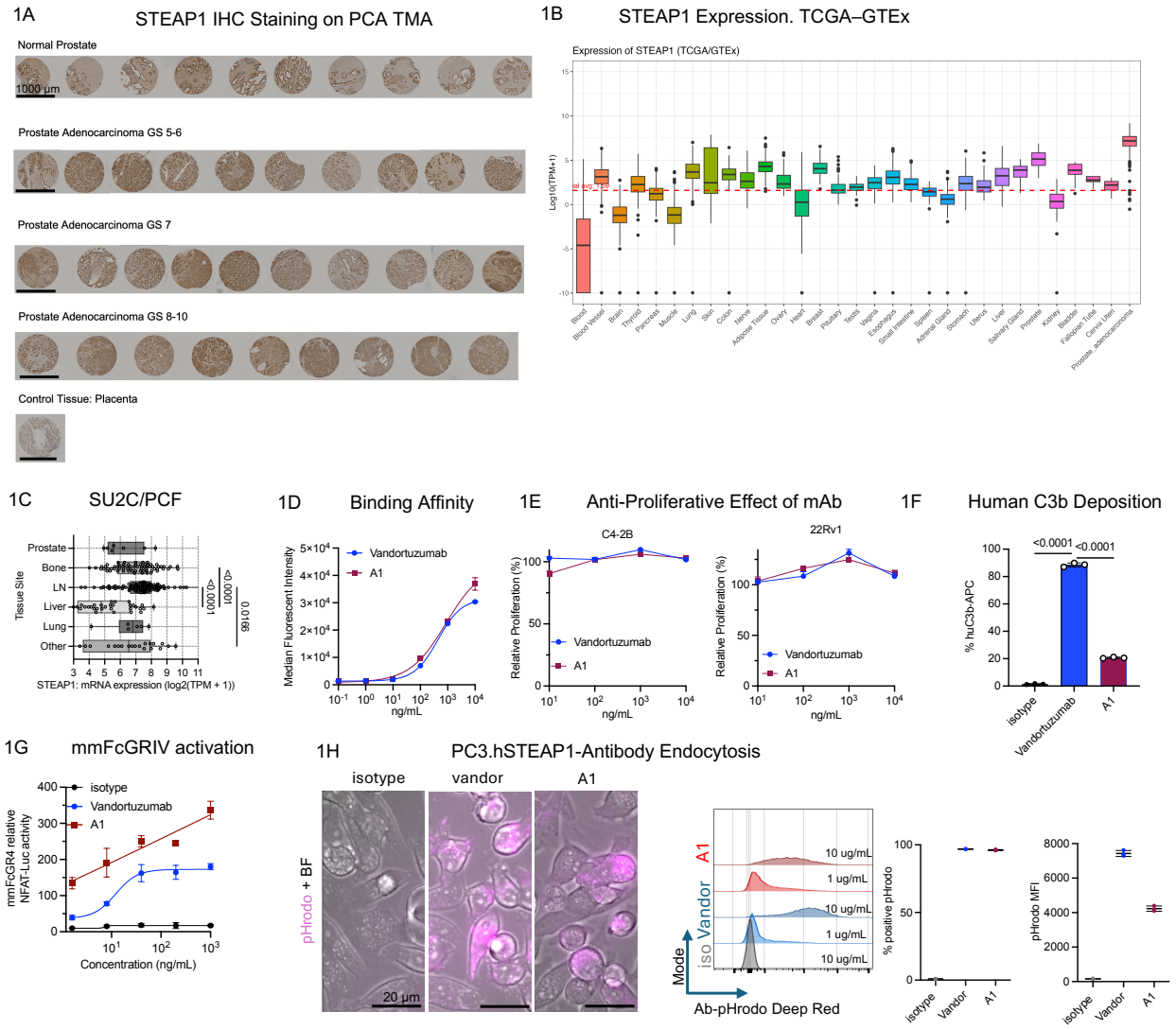

Supplemental Figure 1. Extended STEAP1 expression data and additional antibody characterization. (A) STEAP1 IHC images from TMA, shown as individual tumor cores stratified by Gleason grade category (normal, 5–6, 7, 8–10). Scale bars = 1000 µm. **(B)** STEAP1 mRNA expression (log_2[TPM + 1]) in TCGA Prostate Adenocarcinoma (PRAD) tumor samples and matched normal prostate tissue from GTEx, accessed via UCSC Xena Browser. STEAP1 transcript levels are significantly elevated in tumor relative to normal prostate and other tissue. **(C)** STEAP1 mRNA expression (log_2[TPM + 1]) across metastatic tissue sites (bone, lymph node, liver, lung) in the SU2C/PCF Dream Team mAPMR cohort. Bone and lymph node metastases exhibit the highest median STEAP1 expression; liver and lung metastases show lower and more variable expression. **(D)** Binding affinity of vandortuzumab and A1 on C4-2B STEAP1-positive line, with anti-human AF647 secondary. **(E)** Antiproliferative activity of vandortuzumab and A1 in 22Rv1 (STEAP1-low) and C4-2B (STEAP1-positive) APMR cell lines. Cells were seeded at 3,000 cells per well and cultured for 72 hours prior to viability assessment using the CellTiter-Glo assay. **(F)** human C3b complement deposition on 22Rv1.hSTEAP1 cells measured by flow cytometry (anti-human C3 antibody) following 1 hour treatment with vandortuzumab or A1 in the presence of IgG-

depleted human complement. **(G)** Murine FcγRIV activation by vandortuzumab and A1 assessed by NFAT-Luciferase Jurkat reporter assay. **(H)** Additional internalization data for pHrodo-labeled vandortuzumab or ADC constructs in PC3.hSTEAP1 by flow cytometry and live-cell fluorescence microscopy (CellDiscoverer 7). Data represented as mean ± SD. Statistical analysis for panels **(C)** and **(F)** was performed using one-way ANOVA with Tukey's multiple comparisons test. Dose-response curves in **(D)** and **(G)** were fit using a 4PL model.

Supplementary Figure 2

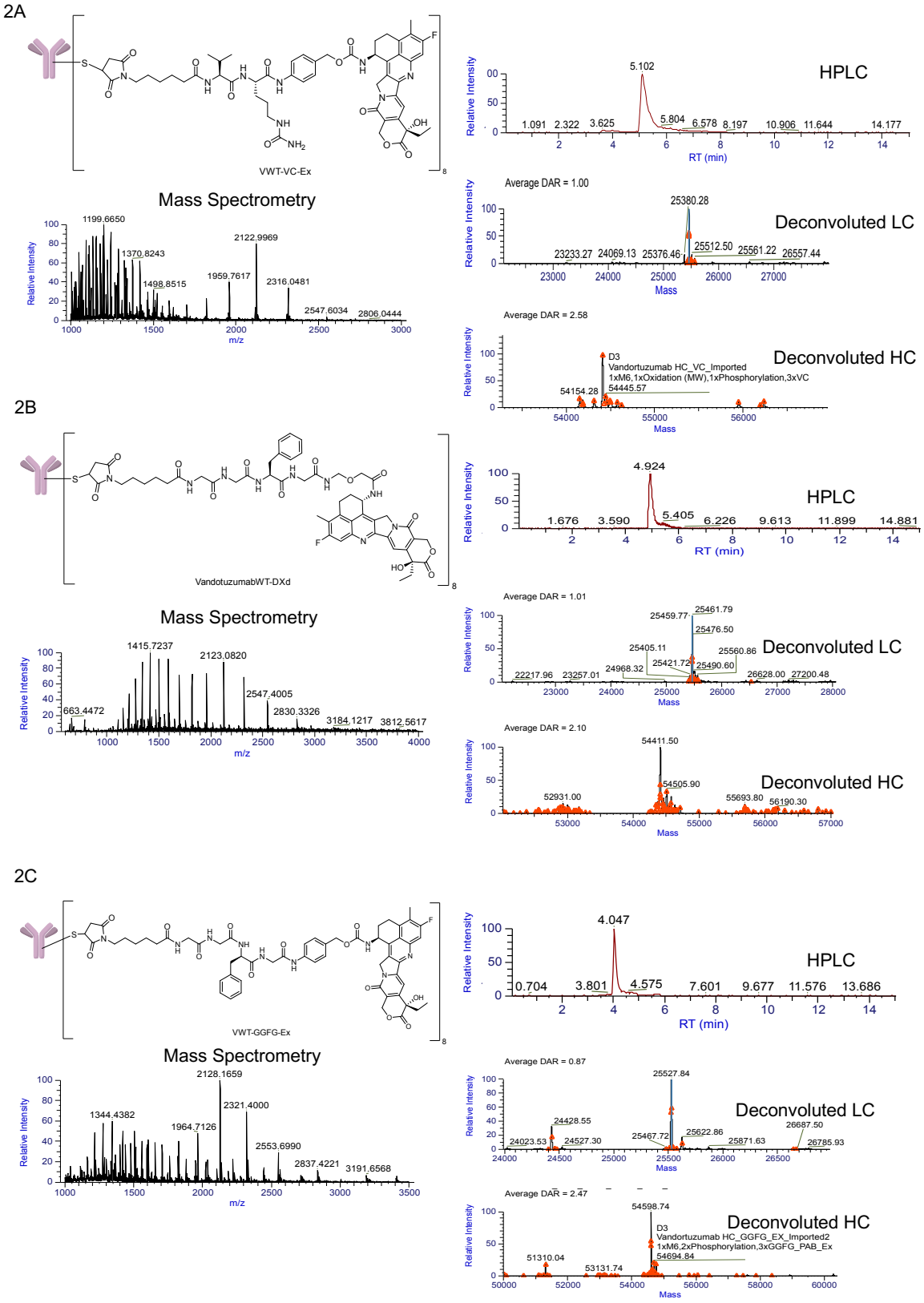

2D

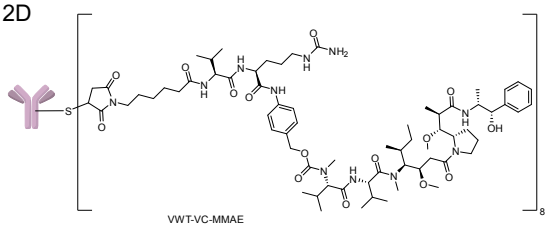
VWT-VC-MMAE

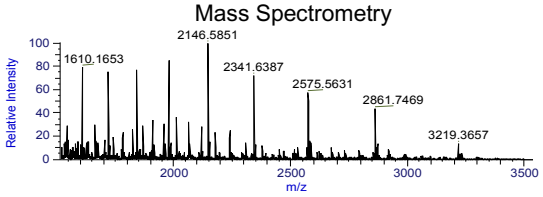
Mass Spectrometry
Relative Intensity
m/z
2146.5851
1610.1653
2341.6387
2575.5631
2861.7469
3219.3657

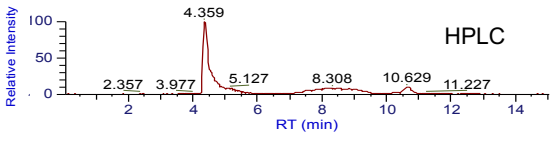
HPLC
Relative Intensity
RT (min)
4.359
2.357
3.977
5.127
8.308
10.629
11.227

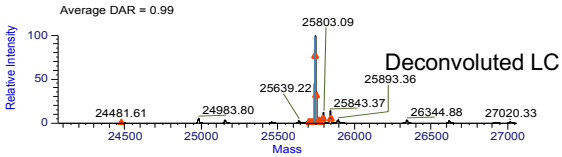
Deconvoluted LC
Average DAR = 0.99
Relative Intensity
Mass
25803.09
25639.22
25893.36
25843.37
24481.61
24983.80
26344.88
27020.33

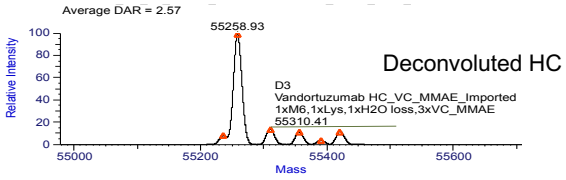
Deconvoluted HC
Average DAR = 2.57
Relative Intensity
Mass
55258.93
D3
Vandortuzumab HC_VC_MMAE_Imported
1xM6,1xLys,1xH2O loss,3xVC_MMAE
55310.41

2E

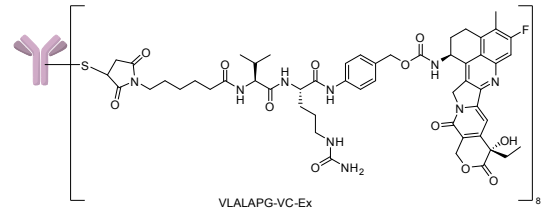
VLALAPG-VC-Ex

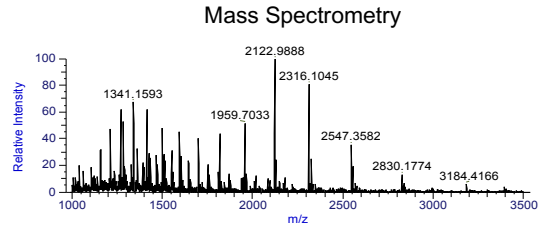
Mass Spectrometry
Relative Intensity
m/z
2122.9888
2316.1045
1341.1593
1959.7033
2547.3582
2830.1774
3184.4166

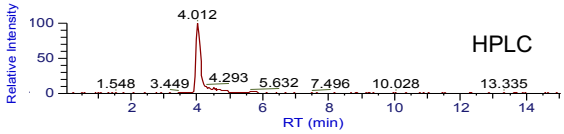
HPLC
Relative Intensity
RT (min)
4.012
1.548
3.449
4.293
5.632
7.496
10.028
13.335

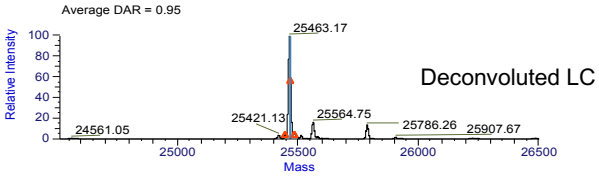
Deconvoluted LC
Average DAR = 0.95
Relative Intensity
Mass
25463.17
24561.05
25421.13
25564.75
25786.26
25907.67

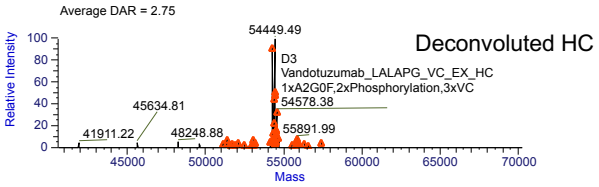
Deconvoluted HC
Average DAR = 2.75
Relative Intensity
Mass
54449.49
D3
Vandotuzumab_LALAPG_VC_EX_HC
1xA2G0F,2xPhosphorylation,3xVC
54578.38
45634.81
41911.22
48248.88
55891.99

2F

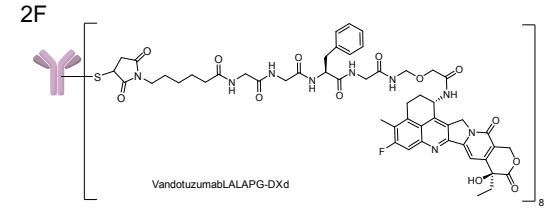
VandotuzumabLALAPG-DXd

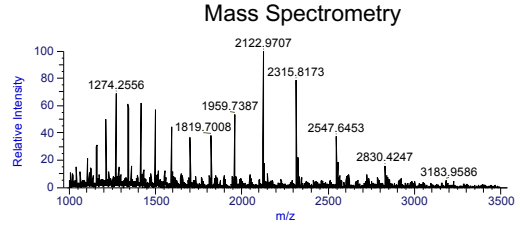
Mass Spectrometry
Relative Intensity
m/z
2122.9707
2315.8173
1274.2556
1959.7387
1819.7008
2547.6453
2830.4247
3183.9586

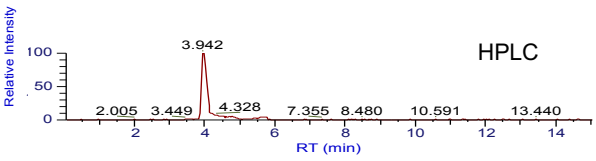
HPLC
Relative Intensity
RT (min)
3.942
2.005
3.449
4.328
7.355
8.480
10.591
13.440

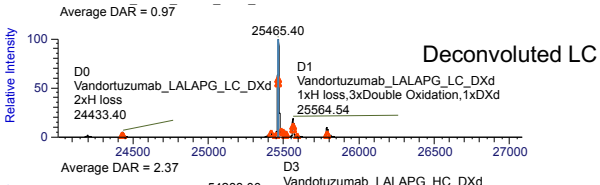
Deconvoluted LC
Average DAR = 0.97
Relative Intensity
25465.40
D0
Vandortuzumab_LALAPG_LC_DXd
2xH loss
24433.40
D1
Vandortuzumab_LALAPG_LC_DXd
1xH loss,3xDouble Oxidation,1xDXd
25564.54

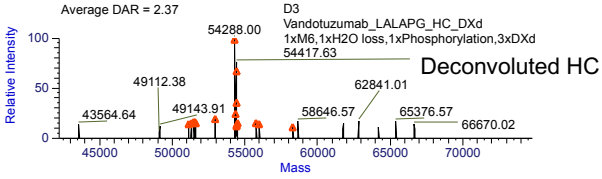
Deconvoluted HC
Average DAR = 2.37
Relative Intensity
Mass
54288.00
D3
Vandotuzumab_LALAPG_HC_DXd
1xM6,1xH2O loss,1xPhosphorylation,3xDXd
54417.63
49112.38
62841.01
43564.64
49143.91
58646.57
65376.57
66670.02

Supplementary Figure 2. Biochemical characterization of vandortuzumab ADC constructs by mass spectrometry and reverse phase high performance liquid chromatography (RP-HPLC). (A-F) (Top left) Chemical structure of each antibody and linker-payload. (Bottom left) High resolution mass spectrum showing multiply charged ions (m/z 2,000–3,500) of denatured ADC used to determine conjugation stoichiometry. (Top right) RP-HPLC chromatogram showing extracted ion chromatogram of intact ADC; (Bottom right) Deconvoluted mass spectrum confirming average drug to antibody ratio on light chain (upper) and heavy chain (lower) and their corresponding masses.

Supplementary Figure 3

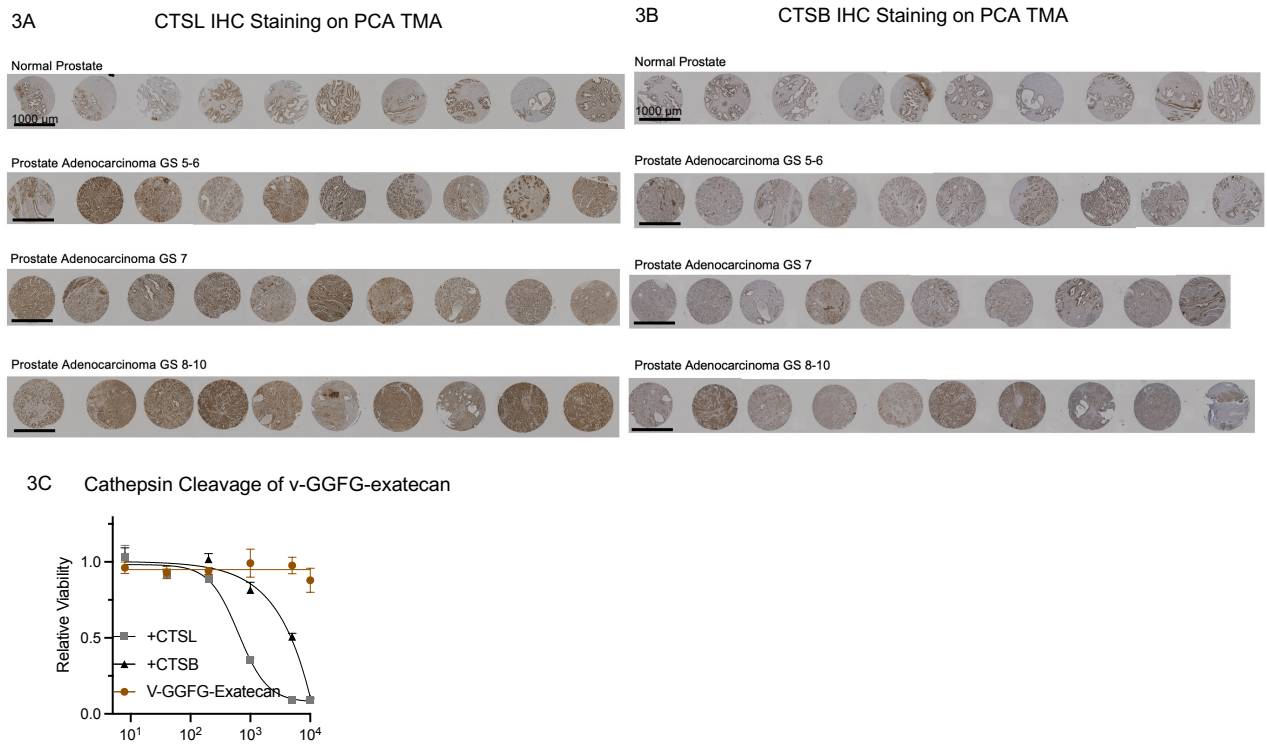

Supplementary Figure 3. Extended cathepsin expression and linker cleavage data. (A-B) CTSL and CTSB IHC images from TMA, shown as individual tumor cores stratified by Gleason grade category (normal, 5–6, 7, 8–10). Scale bars = 1000 µm. **(C)** Cytotoxicity rescue assay for vandortuzumab–GGFG-exatecan (incorporating a PABC spacer). Data in **(C)** represented as mean ± SD. Dose-response curves in **(C)** were fit using a 4PL model.

Supplementary Figure 4

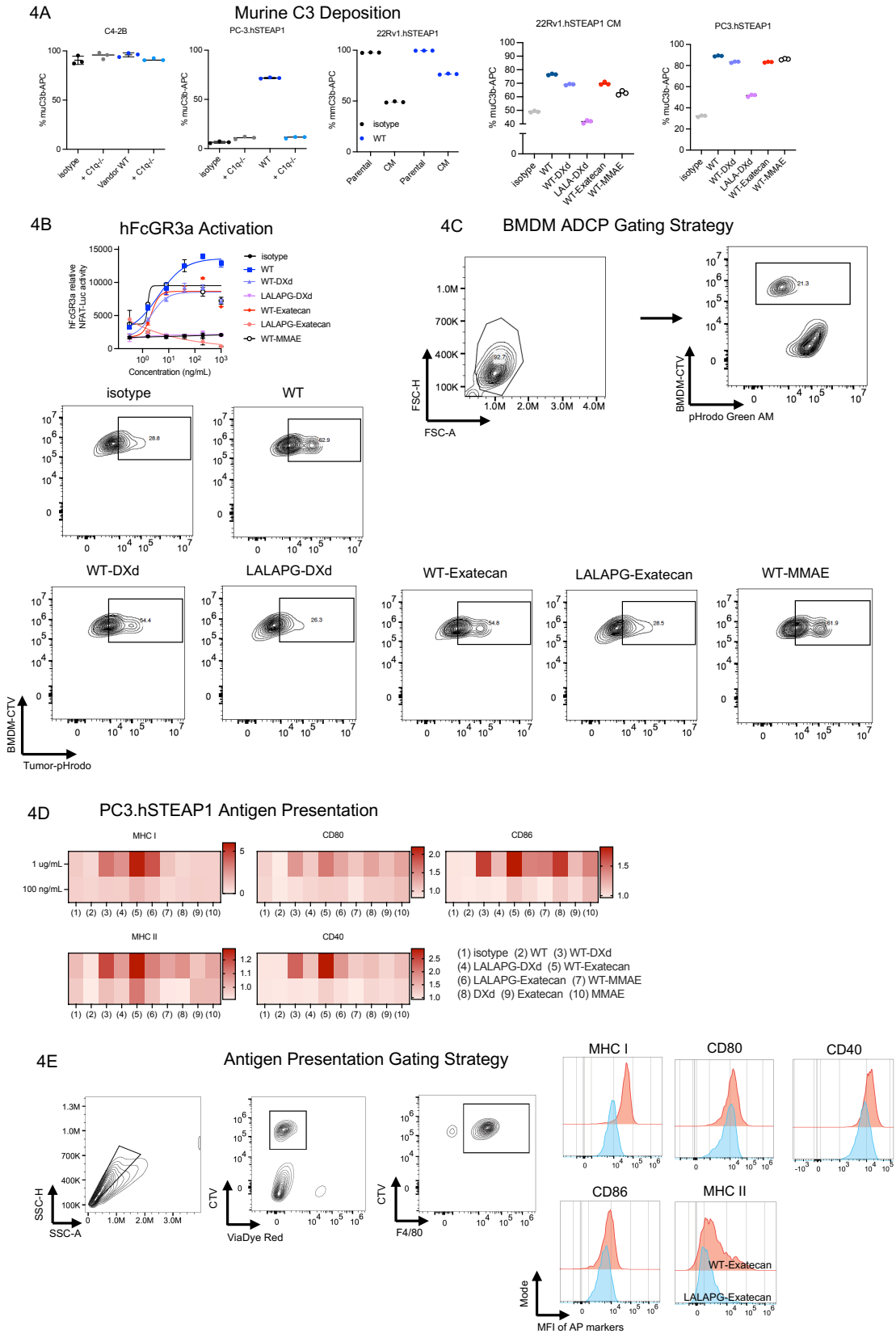

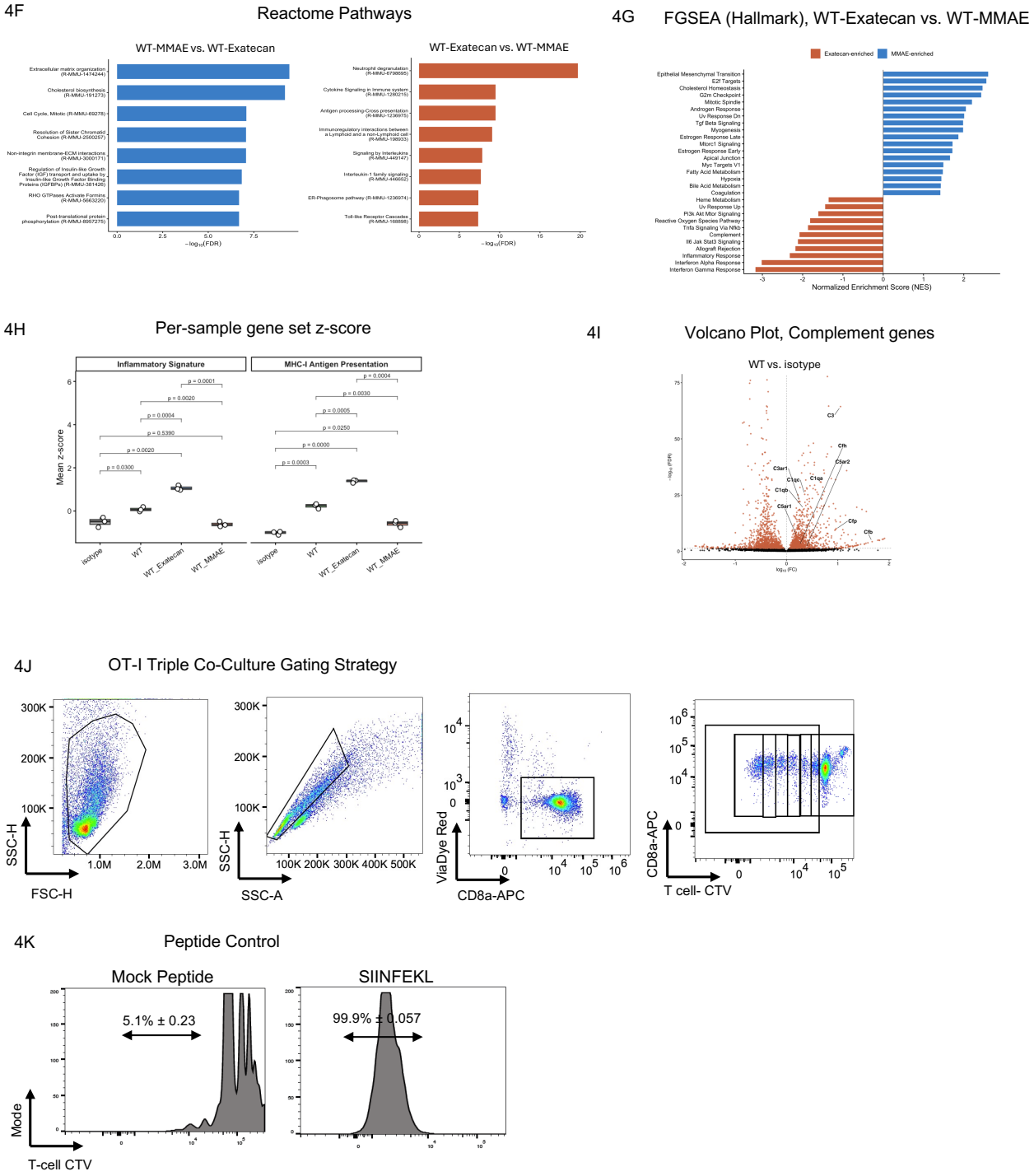

Supplementary Figure 4. Extended characterization of ADC Fc effector functions and ADC-driven innate and adaptive immune activation in vitro. (A) Murine complement deposition across STEAP1-positive cell lines using wild-type or C1q$^{-/-}$ serum. PC3.hSTEAP1 cells demonstrated antibody-dependent, C1q-dependent complement deposition. C4-2B and 22Rv1.hSTEAP1 parental cells showed elevated baseline complement deposition independent of antibody treatment. The caudal metastasis (CM)-derived 22Rv1.hSTEAP1 subline exhibited

antibody-dependent complement deposition with minimal baseline signal. **(B)** Human FcγRIIIA activation assessed by NFAT-Luciferase Jurkat reporter assay. **(C)** Representative flow cytometry gating strategy and quantification for ADCP. Macrophage phagocytosis is shown as the percentage of CellTrace Violet $(CTV)^+$ macrophages that are $pHrodo^+$ following 4-hour co-incubation with pHrodo-labeled tumor cells. **(D)** Antigen presentation marker expression heatmap for BMDMs co-cultured with ADC-treated PC3.hSTEAP1 cells. **(E)** Representative flow cytometry gating strategy for macrophage activation analysis. Macrophages were identified as CTV^+CD11b^+ cells; surface expression of MHC I, MHC II, CD40, CD80, and CD86 was assessed within this gate. **(F)** Reactome pathway enrichment analysis of macrophages co-cultured with vandortuzumab–exatecan– versus vandortuzumab–MMAE–treated tumor cells, each filtered with $\log_2$FoldChange < -0.5. **(G)** Fast gene set enrichment analysis (fgsea) was performed on DESeq2-ranked murine genes using MSigDB Hallmark gene sets. Bars represent the normalized enrichment score (NES); orange indicates gene sets enriched in the WT-Exatecan condition and blue indicates gene sets enriched in the WT-MMAE condition. Only gene sets with adjusted $p < 0.05$ are displayed. **(H)** Mean z-scored expression was computed across curated gene signatures for MHC-I antigen presentation and inflammatory macrophage activation in murine macrophage transcriptomes. Each point represents an individual sample (n = 3 per condition). **(I)** Complement-related transcript expression from bulk RNA-seq of macrophages co-cultured with antibody-treated tumor cells. Vandortuzumab treatment increased expression of several complement components and regulatory transcripts relative to isotype control, suggesting that Fc-mediated complement activation may contribute to macrophage priming. **(J)** Representative flow cytometry gating strategy for OT-I T-cell activation. $CD8^+$ T cells were identified within the live (ViaDye Red^-) gate; CellTrace Violet dilution and CD44 upregulation were used to assess proliferation and activation, respectively. **(K)** Peptide control histograms for OT-I T-cell proliferation. SIINFEKL peptide (positive control, 1 μg/mL) and mock GFP peptide (negative control) are shown. Data in **(A)** and **(B)** represented as mean ± SD. Dose-response curves in **(B)** were fit using a 4PL model. Boxes in **(H)** indicate interquartile range with median line. Pairwise comparisons were performed using Welch's t-test.

Supplementary Figure 5.

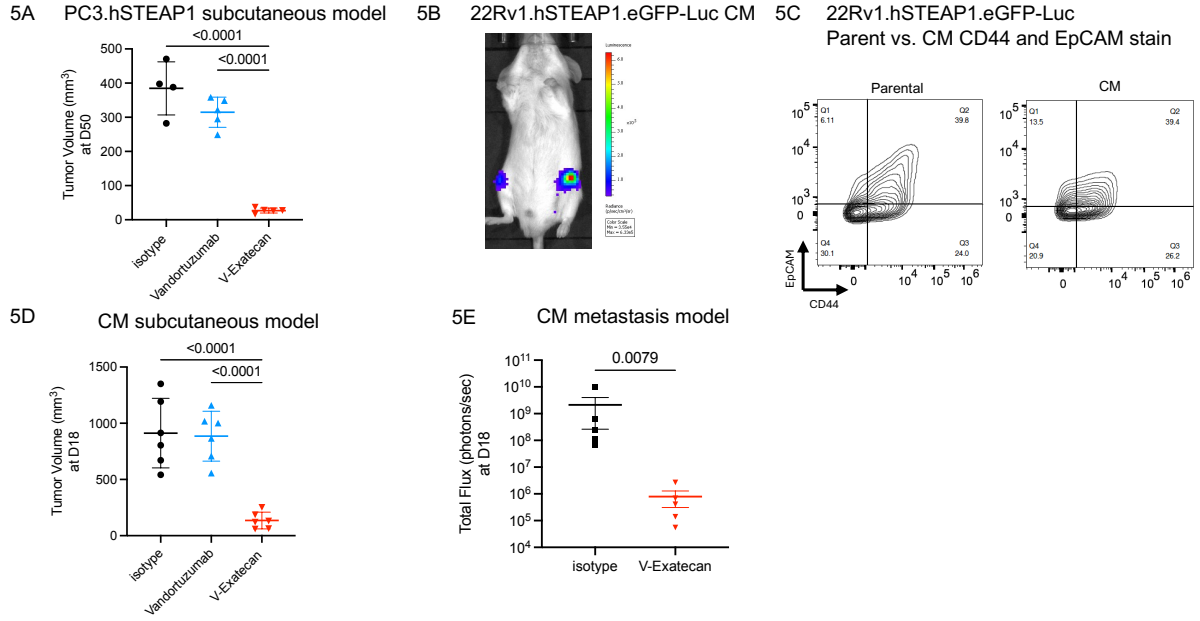

Supplementary Figure 5. Extended in vivo xenograft data and characterization of 22Rv1.hSTEAP1-Luc subline. (A) PC3.hSTEAP1 tumor volume at day 50 following treatment (1 dose of 4 mg/kg isotype, vandortuzumab, or vandortuzumab-exatecan). **(B)** Derivation of 22Rv1.hSTEAP1 CM bone metastasis subline. Bone marrow was flushed from the femur of a tumor-bearing mouse and subsequently re-cultured. **(C)** Flow cytometry analysis of the CM subline suggesting clonal enrichment and loss of the EpCAM^{high} CD44^{high} double-positive population. **(D)** Tumor growth in the 22Rv1.hSTEAP1 CM subcutaneous model at day 18 following treatment (2 doses of 2 mg/kg isotype or vandortuzumab–exatecan). **(E)** Bioluminescent total flux of 22Rv1.hSTEAP1 CM bone metastases at day 18 following treatment initiation (3 doses of 4 mg/kg isotype or vandortuzumab–exatecan). Data represented as mean ± SD. Statistical analyses performed with one-way ANOVA with Tukey's multiple comparisons test (A, D); Welch's t test (E).

Supplementary Figure 6.

6A Expression and in vitro killing of EMT-6.hSTEAP1

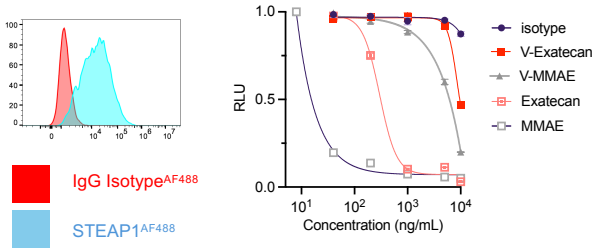

6B Syngeneic EMT6.hSTEAP1 model in BALB/c

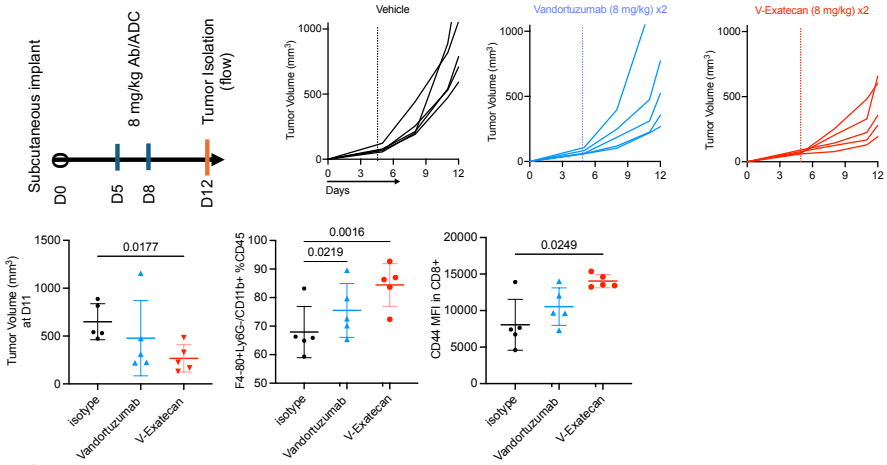

6C Gating Strategy for EMT6.hSTEAP1

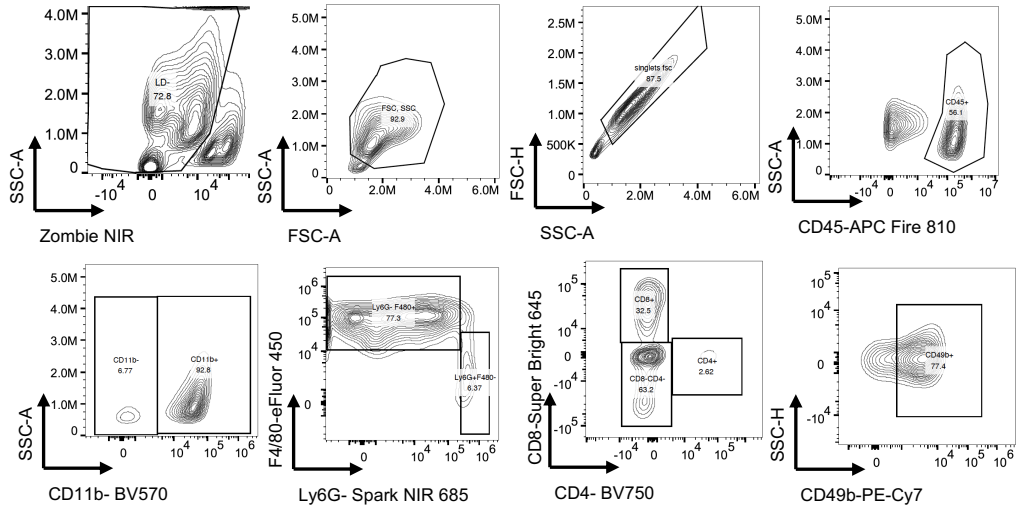

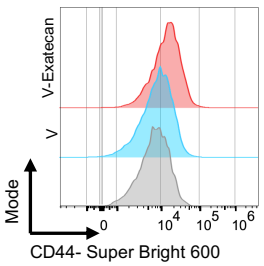

6D CD40 Combination Therapy in EMT6.hSTEAP1

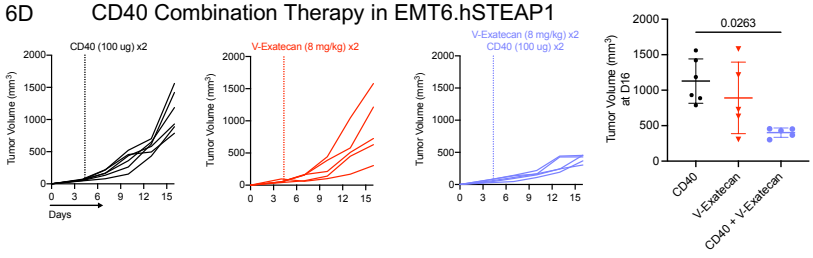

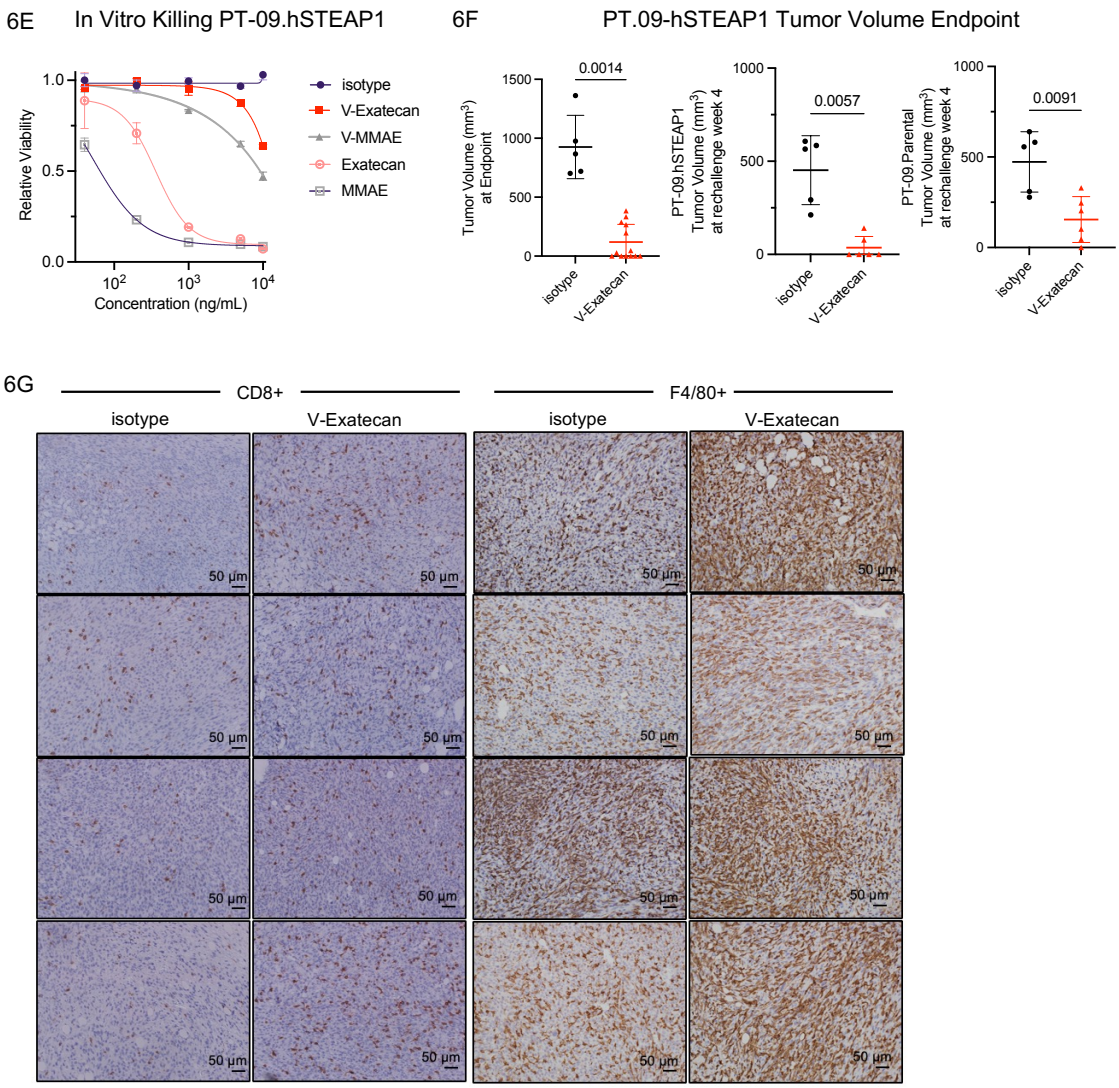

Supplementary Figure 6. EMT-6 syngeneic model data and extended PT-09 characterization. **(A)** Flow cytometry confirming STEAP1 surface expression on transduced EMT-6 cells. In vitro cytotoxicity of EMT-6.hSTEAP1 cells treated with vandortuzumab–exatecan, vandortuzumab–MMAE, and corresponding free payloads following 96-hour incubation, assessed by CellTiter-Glo. **(B)** Schematic of the treatment schedule for the EMT-6.hSTEAP1 syngeneic model. Individual tumor growth curves of EMT-6.hSTEAP1 tumors in BALB/c mice treated with vandortuzumab, vandortuzumab–exatecan, or vehicle control. Vandortuzumab–exatecan reduced mean tumor volume by 41% relative to isotype control (267.1 mm³ vs. 649.5 mm³ at day 11). Post-hoc flow cytometry of intratumoral F4/80^{+}CD11b^{+} macrophages and CD44 MFI on tumor-infiltrating CD8^{+} T cells are shown. **(C)** Representative flow cytometry gating strategy. **(D)** Tumor growth curves for the EMT-6.hSTEAP1 combination study comparing vandortuzumab–exatecan, anti-CD40 agonist, combination therapy, and vehicle control. Combination treatment resulted in greater tumor growth inhibition (mean volume 401 mm³) compared with vandortuzumab–exatecan (891 mm³) or anti-CD40 (1,185 mm³) monotherapy at day 16. **(E)** In vitro cytotoxicity of v–exatecan, v–MMAE, and corresponding free payloads in PT-09.hSTEAP1 cells following 96-hour incubation, assessed by CellTiter-Glo. **(F)** PT-09.hSTEAP1 tumor

volume at initial endpoint (day 34) following treatment with isotype control or v–exatecan. For rechallenge studies, the endpoint was predefined at 4 weeks post-rechallenge. **G)** Representative immunohistochemical images of residual PT-09.hSTEAP1 tumors at day 34 from isotype control– and vandortuzumab–exatecan–treated mice, stained for F4/80 and CD8 across biological replicates. Data represented as mean ± SD. Dose–response curves in **(A)** and **(E)** were fit using a 4PL regression model. Statistical analyses performed with one-way ANOVA with Tukey's multiple comparisons test for endpoint tumor volume in **(B)**, **(D)**, and **(F).**